LOSS ESTIMATE FOR ITER ECH TRANSMISSION LINE INCLUDING MULTIMODE PROPAGATION

M. A. SHAPIRO,[a]* E. J. KOWALSKI,[a] J. R. SIRIGIRI,[a] D. S. TAX,[a] R. J. TEMKIN,[a]
T. S. BIGELOW,[b] J. B. CAUGHMAN,[b] and D. A. RASMUSSEN[b]

[a]*Massachusetts Institute of Technology, Plasma Science and Fusion Center, Cambridge, Massachusetts 02139*
[b]*Oak Ridge National Laboratory, U.S. ITER Project, Oak Ridge, Tennessee 37831*

Received August 7, 2009
Accepted for Publication October 20, 2009

The ITER electron cyclotron heating (ECH) transmission lines (TLs) are 63.5-mm-diam corrugated waveguides that will each carry 1 MW of power at 170 GHz. The TL is defined here as the corrugated waveguide system connecting the gyrotron mirror optics unit (MOU) to the entrance of the ECH launcher and includes miter bends and other corrugated waveguide components. The losses on the ITER TL have been calculated for four possible cases corresponding to having HE_{11} mode purity at the input of the TL of 100, 97, 90, and 80%. The losses due to coupling, ohmic, and mode conversion loss are evaluated in detail using a numerical code and analytical approaches. Estimates of the calorimetric loss on the line show that the output power is reduced by about 5, ±1% because of ohmic loss in each of the four cases. Estimates of the mode conversion loss show that the fraction of output power in the HE_{11} mode is ~3% smaller than the fraction of input power in the HE_{11} mode. High output mode purity therefore can be achieved only with significantly higher input mode purity. Combining both ohmic and mode conversion loss, the efficiency of the TL from the gyrotron MOU to the ECH launcher can be roughly estimated in theory as 92% times the fraction of input power in the HE_{11} mode.

KEYWORDS: *ITER, electron cyclotron heating, transmission line*

Note: Some figures in this paper are in color only in the electronic version.

I. INTRODUCTION

I.A. ITER ECH/ECCD System

Electron cyclotron heating (ECH) and electron cyclotron current drive (ECCD) in ITER will be provided by twenty-four 1-MW, 170-GHz gyrotrons.[1] Figure 1 is a schematic of the ECH/ECCD system of ITER (Ref. 2). The transmission line (TL) connects the gyrotron system to the ECH launcher (equatorial launcher and upper launchers).[3–5] The ITER requirement for the efficiency of the TLs is governed by the specification that a total power of 20 MW should be delivered to the plasma out of the 24 MW generated by the gyrotrons. Therefore, the efficiency of the ECH system including all the components from the gyrotron window to the plasma should be 83%. Since the ECH system contains many complex components and presents a long transmission length, it is a challenge to meet the ITER requirement on transmission losses. The efficiency of TLs that carry megawatt power level gyrotron radiation is a topic of intensive present-day research.[6–15]

Figure 2 presents a schematic of the TL connecting the gyrotron to the equatorial launcher. The gyrotron output radiation is transmitted and converted by the mirror optics unit (MOU) for coupling to the corrugated waveguide.[6] The microwave power is transmitted using 63.5-mm-diam corrugated waveguides. Along with the straight waveguide sections and miter bends (MBs), the TL contains polarizers (combined with the MBs), valves, direct-current breaks, pumping sections, releasers, and other components. The TLs for the ITER ECH system are still under design, and the schematic shown in Fig. 2 should be understood as an example of the configuration. The final configuration may be different.

In this paper we define the ITER TL as all waveguide components from the MOU output to the ECH launcher entrance. Waveguide components from the diamond

*E-mail: shapiro@psfc.mit.edu

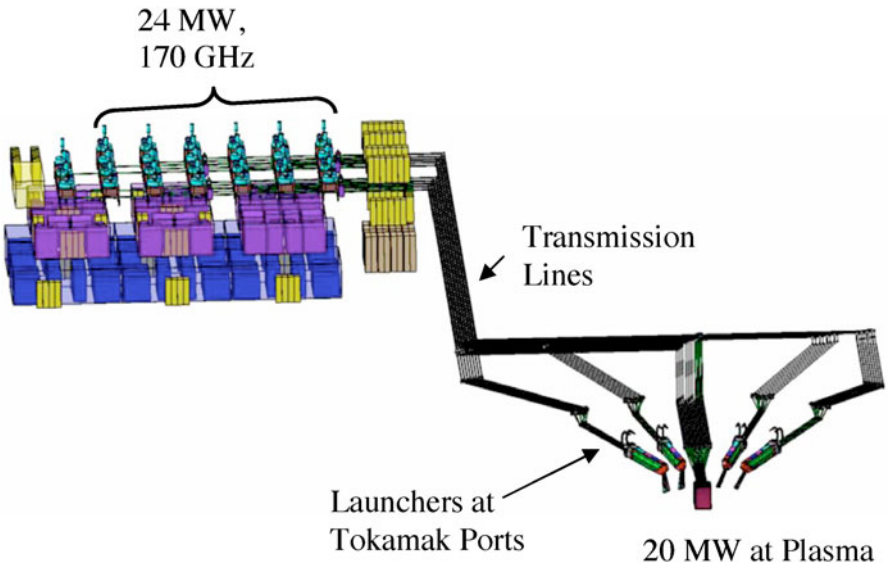

Fig. 1. Schematic of ITER ECH system.[2]

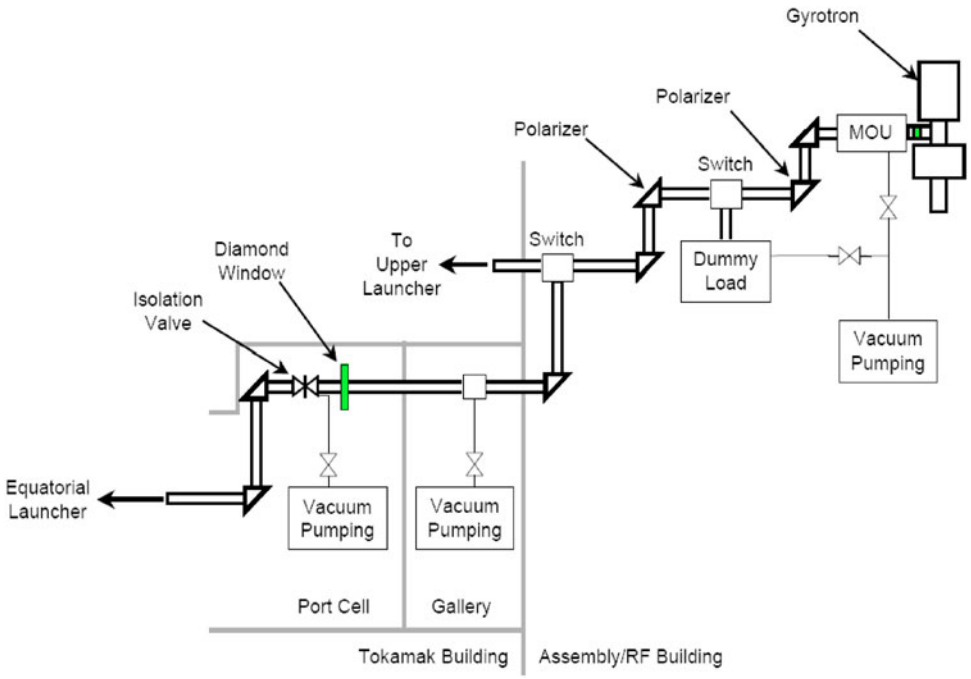

Fig. 2. Schematic of the ITER TL to the equatorial launcher.

window onward to the plasma are with the ECH launcher. The efficiency of the TL should exceed 83% to allow some loss in the ECH launcher and MOU. The TL contributes the largest fraction of losses but not the entire 17%.

The HE_{11} mode of a corrugated waveguide is the operating mode of the TL. The TL provides extremely low ohmic loss of the HE_{11} mode in the straight waveguide sections. Mode conversion losses of the HE_{11} mode occur primarily in the MBs, gaps, and other components. In some previous research on ECH TLs, it has been assumed that the mode excited at the entrance of the line is a pure HE_{11} mode. However, research shows that gyrotron beams coupled onto the TL often excite high-order

modes (HOMs) in addition to the fundamental HE_{11} mode. The excitation of HOMs is caused by imperfections in the Gaussian-like beam from the gyrotron (phase errors, incorrect waist size, etc.) as well as coupling errors of the beam into the guide (tilt, offset).[16] The purpose of this paper is to calculate the losses on the ITER ECH TL for realistic cases that include HOM excitation on the TL.

This paper presents an estimate of the losses for four cases of power transmission in the ITER ECH TL. The four cases represent different levels of the efficiency of excitation of the fundamental HE_{11} mode in coupling of the microwave beam from the gyrotron onto the ECH line.

I.B. Representative ITER TL Components

The design of the ITER TL is still ongoing.[2] For the present calculations, our goal is an understanding of the role of HOMs in the power transmission and the mode conversion on the TL. Therefore, we have used an available, older model of the TL, which is described in Table I. The present results are illustrative of the calculation methods and can be easily refined as the TL design changes. Changes in the design of the TL will change the numerical results but should not change the conclusions of this study.

The parameters in Table I were taken from the 2007 ITER design for the TL to the equatorial ECH launcher. Nine waveguide sections and eight MBs are used in this TL (Table I). Two MBs serve as polarizers. In this calculation, we include the possibility that the MB mirrors have small fabrication errors, amounting to a tilt of ± 0.025 deg. The tilt is entered by specifying the specific values shown in Table I. Introduction of this tilt will result in some mode conversion. A 20-μm bulge of the MB mirrors due to heating was calculated, but its effect on the performance of the MB was found to be insignificant.

TABLE I

ITER Waveguide and MB Parameters

Waveguide Section/ MB Number	Waveguide Length (m)	MB Mirror *X*/*Y*-Plane Tilt (deg)	Polarizer
1	1.2	0.025/−0.025	No
2	22	−0.025/0.025	Yes
3	40	0.025/−0.025	Yes
4	9.1	0.025/−0.025	No
5	8	−0.025/0.025	No
6	11	−0.025/0.025	No
7	20	0.025/−0.025	No
8	2.9	−0.025/0.025	No
9	8.8		

II. LINEARLY POLARIZED LP_{mn} MODES OF CORRUGATED WAVEGUIDE

The present work differs from previous approaches in the exclusive use of linearly polarized modes (LP_{mn}, m is the azimuthal index, and n is the radial index) to describe the modes excited on the TL. The beam from the gyrotron is usually close to 100% linearly polarized. This microwave beam will excite the linearly polarized modes (LP_{mn} modes) of the waveguide. The LP_{11} modes of the corrugated metallic waveguide were first discussed in Ref. 17, where it was shown that the LP_{11} modes could be constructed from the usual eigenmodes of the corrugated waveguide. The set of LP_{mn} modes may be used in a corrugated waveguide if the corrugation depth is a quarter of a wavelength.

Linearly polarized modes LP_{mn} can be constructed as a superposition of the HE, EH, TE, and TM modes of a corrugated waveguide. The transverse electric field in the LP_{mn} modes can be expressed as follows (for polarization along the y-axis):

$$\vec{E}_{mn}^{\perp} = \frac{X_n}{a} J_m\left(X_n \frac{r}{a}\right)\cos(m\phi)\,\hat{y}\ (\mathrm{LP}_{mn}\ \text{even mode})$$

and

$$\vec{E}_{mn}^{\perp} = \frac{X_n}{a} J_m\left(X_n \frac{r}{a}\right)\sin(m\phi)\,\hat{y}\ (\mathrm{LP}_{mn}\ \text{odd mode})\ , \tag{1}$$

where

(r, ϕ) = polar coordinates

a = waveguide radius

X_n = n'th zero of the Bessel function J_m.

Note that the LP_{0n} modes are the same as the HE_{1n} modes, and we use the latter notation in this paper.

In this paper we consider only linearly polarized waves in the TL. A circularly polarized wave is the superposition of two linearly polarized waves, which are not coupled in the conventional MBs and other TL components. Therefore, the losses for circularly polarized waves can be estimated as a sum of the losses for a 50% mixture of power in the two polarizations.

The power in HOMs at the output of the TL may be inefficiently radiated by the ECH launcher. This power may reach the plasma and be absorbed through ECH, but this ECH absorption is not quantitatively estimated and is considered as power loss.

III. TL LOSS: OVERVIEW

The loss on the ITER TL consists of three components:

1. coupling loss
2. ohmic loss
3. mode conversion loss.

The first component of loss is the coupling loss. It occurs when the microwave beam from the gyrotron couples to the HE_{11} mode of the TL with $<100\%$ efficiency. The second component of loss is ohmic loss. This loss occurs when modes are absorbed along the TL. The coupling loss and ohmic loss can be combined as the calorimetric loss. The third component of loss is mode conversion loss. Mode conversion at MBs, gaps, and other components results in power exiting the TL in modes other than the desired HE_{11} mode. These different loss mechanisms are taken into account in the loss calculations presented in this paper.

If the MOU output is a Gaussian beam (GB), the coupling into the HE_{11} mode at the waveguide aperture is not 100% efficient. The coupling loss associated with the beam truncation and mode conversion can be reduced by using a specially designed taper, which is a converter of the TEM_{00} mode (GB) to the HE_{11} mode. Such a mode converter was studied in Refs. 18 and 19 and utilized in a low diffraction MB (Ref. 8).

III.A. Coupling of Power into the ITER TL

The technology of creating a high-mode purity beam from the gyrotron and then perfect coupling to the waveguide is not available today. There is a great uncertainty, and rather than trying to quantify this value, we have chosen a different approach and consider four cases: one case of pure HE_{11} mode excitation and three cases that cover more realistic situations. Case 1 is excitation of a 100% pure HE_{11} mode at the entrance of the TL. This case does not include GB coupling and is considered for purposes of comparison. The three realistic cases with GB coupling are case 2, perfect coupling of the GB to the TL; case 3, more realistic expectation; and case 4, worst case (hopefully).

The output beam from the gyrotron MOU is assumed to be a slightly imperfect GB containing 1 MW of power. We allow some variation in waist size and beam tilt. The four examples of mode excitation of the corrugated waveguide are presented in Table II. These coupling examples differ by the HE_{11} mode power excited in the waveguide. The percentage of the HE_{11} mode varies when the GB parameters change (the beam waist size, tilt angle, or beam offset). The cases labeled 2, 3, and 4 are only representative values. For example, it is possible to construct another version of case 3, with 90% efficiency of excitation of the HE_{11} mode, using different values of the GB waist, tilt, etc.

The coupling of a GB into a corrugated waveguide has been calculated in detail by Ohkubo et al.[16] It is shown in Ref. 16 that the coupling efficiency is more sensitive to the tilt angle than to the beam ellipticity or offset. The HE_{11} mode content for the four cases in Table II is mostly determined by the tilt. The ellipticity and offset are added to include all possibilities. Experimentally, it is more difficult to provide beam alignment with respect to the waveguide. We have written a code to calculate the coupling of the field of the GB onto the LP_{mn} modes of the corrugated waveguide. We also take into account a small truncation loss that arises because a small portion of the GB is outside of the 63.5-mm waveguide aperture. This truncation amounts to an $\sim$1% reduction in power coupled onto the TL for cases 2, 3, and 4 of Table II. Since we have assumed that the GB from the gyrotron has 1 MW of power, this truncation loss will be treated as equivalent to ohmic loss in the calculations that are presented in this paper.

The maximum coupling efficiency of the ideal GB (100% TEM_{00} mode) to the HE_{11} mode on the TL is 98% (Ref. 16). Cases 2, 3, and 4 can be respectively translated to having 99.3, 91.5, and 82% of the power in the ideal TEM_{00} mode before coupling to the TL.

III.B. Ohmic Loss

Ohmic loss occurs in transmission through the straight sections and in reflection from mirrors or polarizers at the MBs. A detailed calculation of the ohmic loss in the straight sections has been given recently by Doane,[9] and we have used his estimate in Table III. The ohmic loss at an MB is given by

TABLE II

Examples of Coupling of a GB onto the TL

Coupling Example	Case	GB Waist in *Y*/*X* Direction W0 (*y*/*x*) (cm)	GB Tilt in *Y*/*X* Direction (deg)	GB Offset in *Y*/*X* Direction (cm)	Fraction of Input Power in the HE_{11} Mode (%)
100% HE_{11}	1	2.03/2.03	0/0	0/0	100
97% HE_{11}	2	2.08/1.98	0.07/0.07	0.07/0.07	97
90% HE_{11}	3	2.18/1.98	0.3/0.3	0.1/0.2	90
80% HE_{11}	4	2.18/1.98	0.45/0.5	0.1/0.2	80

TABLE III

Ohmic Loss Parameters

Straight section HE_{11} mode Ohmic loss [decrement (Np/m)]	0.18×10^{-4}
MB mirror ohmic loss (fractional)	0.14×10^{-2} (without polarizer)/0.28×10^{-2} (with polarizer)

$$Loss = (1.2) \times 4 \frac{R_s}{Z_0} \begin{bmatrix} \cos\alpha \\ 1/\cos\alpha \end{bmatrix} \begin{matrix} H\text{-}Plane \\ E\text{-}Plane \end{matrix}, \qquad (2)$$

where

R_s = surface resistance

$Z_0 = 377\ \Omega$ = impedance of free space

α = incidence angle.

A factor of 1.2 is added to Eq. (2) because of surface roughness[9] and is used in this calculation. The surface roughness correction may be higher; a value as high as 1.5 was reported in Ref. 20.

For room temperature copper, the loss is 0.10% for an H-plane bend and 0.19% for an E-plane bend. For convenience, we use a weighted average value of 0.14% for each bend in the TL. The loss at the polarizers is estimated as double that of a conventional bend [factor of 2.4 in Eq. (2)] (Ref. 9). However, the loss can be a factor of 4 higher than the theoretical loss for a plane mirror according to Ref. 21 [factor of 4 in Eq. (2)]. The ohmic loss parameters for the waveguide straight sections and MB mirrors are listed in Table III.

In this paper, we calculate the losses for a linearly polarized wave transmission and use the average value for ohmic loss. The results can be used for the circularly polarized wave as well assuming that 50% of the power is in the E-polarization and 50% is in the H-polarization.

III.C. Simulation of Loss due to Diffraction in an MB

Diffraction at an MB leads to the excitation of HOMs at the output port of the bend. This loss has been previously estimated by Doane and Moeller.[22] However, their results were obtained exclusively for the HE_{11} and TE_{01} modes. We have extended that theory to estimate the loss for higher-order LP_{mn} modes. However, we have found it to be more convenient to develop a completely new code to simulate mode conversion and losses in an MB and have used our code in analyzing the ITER ECH TL.

Our propagation code simulates mode conversion in MBs for an arbitrary input mode mixture. The ability to treat a mixture of modes is important because the gyrotron output radiation excites a mixture of modes in the corrugated waveguide, not a pure HE_{11} mode. The code calculates the mode mixture at the exit port of an MB for any input of a sum of LP_{mn} modes of arbitrary relative phase. Power converted into HOMs is tracked in the calculation for the first 110 LP_{mn} modes of the waveguide (10 axially symmetrical modes LP_{0n} and 10×10 nonsymmetrical modes), which is sufficient for the accuracy needed in this calculation (99.9% of the total power was in these 110 modes).

The code is based on a fast Fourier transform (FFT) calculation advancing the fields through the MBs. Straight sections are calculated analytically. The FFT code was developed to simulate field propagation in the equivalent circuit of an MB (Fig. 3). The equivalent circuit includes two semi-infinite circular waveguides with the apertures formed by two miter cuts (Fig. 3b). For this circuit, the power radiated from one waveguide and not captured by the other waveguide is considered as loss. The mode content in the receiving waveguide can be calculated. The mode conversion loss can be determined from the comparison of mode contents in the input and output waveguides. Another way to represent the equivalent circuit of an MB is a waveguide cross (Fig. 3c) (Ref. 23). It is similar to the two waveguides with miter cuts at the ends. However, the waveguide cross is a closed circuit; therefore, the power loss is in the modes excited in the transverse arms of the waveguide cross. If we assume that the waveguide walls are thick (Fig. 4a), we can form the cross sections of transition from the input to the receiving waveguide in the waveguide cross (shown in Fig. 4b).

The method of the FFT calculation is based on the calculation of the field in a square box whose dimensions are larger than the size of the circular guide. Figure 4b shows the sequence of cross sections used in the FFT simulation. At the beginning of the calculation, the field

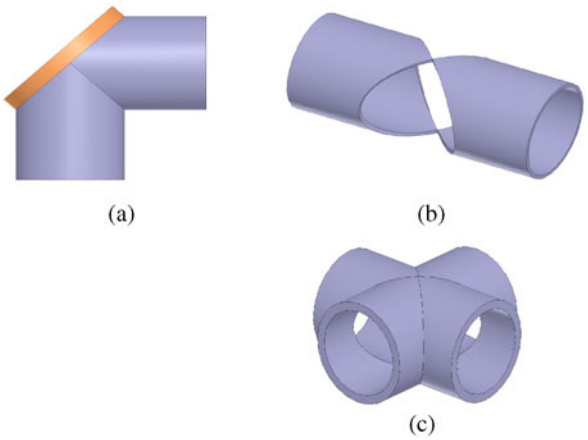

Fig. 3. (a) The MB and its equivalent circuits; (b) two waveguides with miter cuts; (c) waveguide cross.

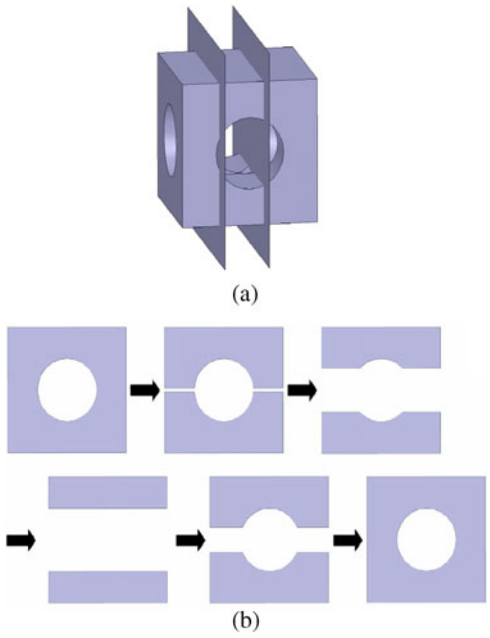

Fig. 4. (a) Illustration of waveguide cross and cross sections; (b) waveguide cross-section variation used for FFT simulation of the MB equivalent circuit (Fig. 3).

of the LP_{mn} mode is confined to the 63.5-mm circular aperture and is zero outside the circular aperture. The code calculates the field progressively along the direction of the waveguide. The outer square aperture remains constant, but the cross section of the inner waveguide varies from a circular to a rectangular aperture and back (Fig. 4b).

The field is represented by the superposition of modes of the square area with sides L in Cartesian coordinates:

$$A(x,y)\exp(j\varphi(x,y)) = \sum D_{pq} \sin\left(\frac{p\pi x}{L}\right)\sin\left(\frac{q\pi y}{L}\right) , \tag{3}$$

where $A(x,y)$ is the linearly polarized field amplitude and $\varphi(x,y)$ is the phase. The coefficients D_{pq} are determined by applying an FFT.

As previously mentioned, the fields within the metal region of the cross section must be identically zero. This will be the case for each cross section; however, we note that the fields will be allowed to have a nonzero magnitude within the slots on the sides. Let us now explore how the fields are propagated at each step. The propagation distance for each step will be $\Delta z = 2a/N$, with N being the total number of steps to cross the gap region. Recall that the fields are represented as a series of modes of the square cavity, shown in Eq. (3). The propagation constant for each mode is therefore defined as

$$k_{z,pq} = \sqrt{k^2 - \left(\frac{p\pi}{L}\right)^2 - \left(\frac{q\pi}{L}\right)^2} , \tag{4}$$

where $k = \omega/c$ is the wave number. We now propagate these fields by one step:

$$A\exp(j\varphi)_{(1)} = \sum D_{pq} \sin\left(\frac{p\pi x}{L}\right)\sin\left(\frac{q\pi y}{L}\right) \times \exp(jk_{z,pq}\Delta z) . \tag{5}$$

The new field amplitude should be zeroed out if it falls into the shaded region (Fig. 4) at the new cross section. To account for this, we take the inverse FFT of the series of modes, returning to the domain of an array of field amplitudes and phases. We define a new amplitude $\tilde{A}_{(1)}\exp(j\varphi)$ that has been truncated by the shaded region. The fractional loss due to truncation from propagating across the first step is

$$T_1 = \frac{\int A_{(1)}^2\, dxdy - \int \tilde{A}_{(1)}^2\, dxdy}{\int A_{(1)}^2\, dxdy} . \tag{6}$$

We then take $\tilde{A}_{(1)}\exp(j\varphi)$, and as was the case with our initial function, we represent it as a series of modes of the square box by taking the FFT. This function is then propagated to the next cross section where we take the inverse FFT, truncate the fields, and calculate the loss once again. This process is repeated step-by-step until the whole gap region has been traversed and we obtain a final function $\tilde{A}_{(N)}\exp(j\varphi)$. This final function is then decomposed into a series of LP_{mn} modes of the corrugated waveguide. For the calculations presented here, the number of steps N is 200, and the size of the calculation region, the square of side L, is $L = 127$ mm. Increasing N or L does not significantly change the results of the calculation; varying N or L by 10% results in 3 to 4% variation in the loss.

The final result of each simulation can be broken down into three components: HE_{11} mode transmission; output power appearing at the output port in HOMs; and a truncation loss of power that does not reach the output port, that is defined as

$$T_{GAP}\,(\mathrm{dB}) = \sum_{n=1}^{N} T_n\,(\mathrm{dB}) , \tag{7}$$

where the fractional loss Eq. (6) is converted to decibels.

To validate the FFT code, we have calculated the loss in an axially symmetrical gap of length $2a$ in a corrugated waveguide of diameter $2a$ for the HE_{11} mode using this new approach and compared the results with the Doane and Moeller theory.[22] The agreement for two examples, shown in Table IV, is excellent.

TABLE IV

Calculation of Loss in a Waveguide Gap of Length 2*a*

Waveguide Diameter (2*a*) and Frequency	Gap Loss (Ref. 22)	Gap Loss (This Calculation)
63.5-mm diameter/170 GHz	0.022 dB	0.022 dB
31.75-mm diameter/110 GHz	0.120 dB	0.125 dB

The diffraction in the nonsymmetrical gap shown in Fig. 3b results in two distinct loss mechanisms:

1. mode conversion into HOMs in the receiving port. The HOMs, which are excited in the receiving port, are often capable of propagating down the TL. They do not induce large ohmic loss near the MB.
2. radiation from the input port that misses the output port. In a closed MB geometry (Fig. 3a), the radiation that misses the receiving port excites very high order modes (VHOMs). These VHOMs are close to cutoff in a highly overmoded waveguide and are dissipated through ohmic losses in the waveguide within a few meters of the MB.

Table V contains the results of MB diffractive loss calculations for two MBs: the ITER 170-GHz MB and the General Atomics 110-GHz MB. The results shown for the theory[22] are obtained from an axially symmetrical gap calculation. Doane and Moeller[22] argue that the loss in an MB is one-half the loss in a gap of length 2*a* since the diffraction effect is the same in both cases, but in the MB one-half of the wall is covered by a waveguide (see Ref. 22). The entries for the Doane and Moeller[22] calculation in Table V are obtained by taking one-half of the loss from the gap calculation shown in Table IV. The FFT calculations of the MB loss (Table V) agree reasonably well with Ref. 22. Table V indicates that the ITER MB, more oversized than the General Atomics MB, can be more accurately estimated by the Doane and Moeller[22] theory. The percentage of loss due to mode conversion into VHOMs is also given in Table V from the FFT code. The VHOM power is estimated from the power that does not reach the output port. This code may also be used when the field at the input port is a mixture of waveguide LP_{mn} modes. In that case, if two modes are present at the input port with the same symmetry (the same *m* value, but different *n* values), the modes will interfere at the output port. The resulting mode conversion in the MB will be a function of the relative phase of the two modes at the input port.[24] With 2% of the power in the HE_{12} mode, the loss can be higher by 0.01 dB per MB (Ref. 24). Our code naturally incorporates this effect. Since the relative phase at subsequent MBs will depend on the exact distance separating the bends, the effect depends strongly on the exact design of the ITER TL. When averaged over a large number of MBs, it is hoped that the relative phase will tend to be somewhat random, thus minimizing this effect.

In addition to the loss caused by diffraction, there will also be MB loss caused by ohmic loss on reflection from the MB mirror; diffraction loss if the MB mirror is tilted away from exactly 90 deg, etc. These additional losses are taken into account in the calculation of total loss in the ITER TL.

IV. LOSS ON THE ITER TL: RESULTS FOR A PURE LP_{mn} MODE

We first consider the transmission of individual, pure LP_{mn} modes on the ITER ECH TL. The ITER TL parameters used in these calculations are given in Table I. Figure 5 shows loss calculation results for the lowest-order modes propagating in the ITER corrugated waveguide TL. The calculated losses include the following:

1. MB mode conversion loss into VHOMs. These modes are forward and backward modes (see Ref. 22). They are trapped in the waveguide near the MB and dissipated through ohmic loss.
2. ohmic loss (Table III) in the straight waveguide sections
3. ohmic loss in the MB mirror (Table III)
4. loss due to mode conversion to other modes, which are HOMs that transit the TL to the output port.

TABLE V

MB Loss

MB Parameters	MB Loss (Ref. 22)	MB Loss (This Calculation)	Percentage of Loss to VHOMs (This Calculation)
170 GHz/63.5-mm diameter	0.011 dB	0.013 dB	47%
110 GHz/31.75-mm diameter	0.060 dB	0.085 dB	56%

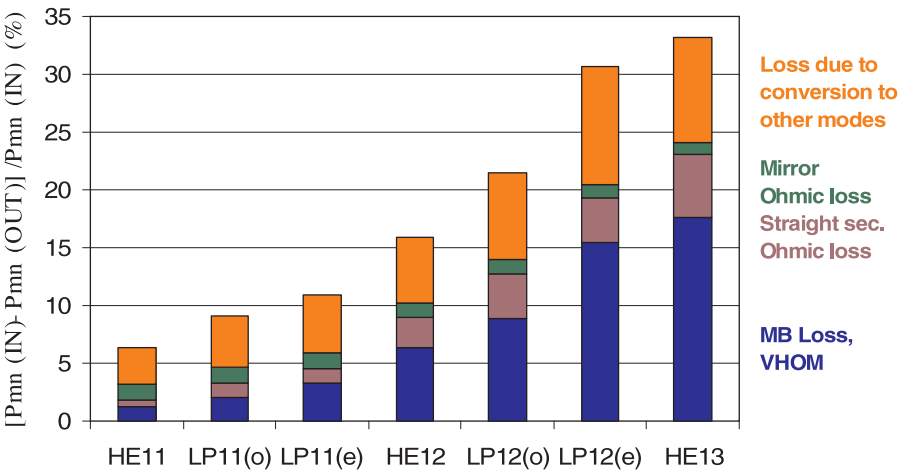

Fig. 5. Loss (%) in the ITER TL for pure mode input. Partitions: (1) loss in the miter bends due to excitation of VHOMs that add to ohmic loss; (2) ohmic loss in straight sections; (3) ohmic loss in the MB mirrors; (4) loss due to mode conversion to power in other modes.

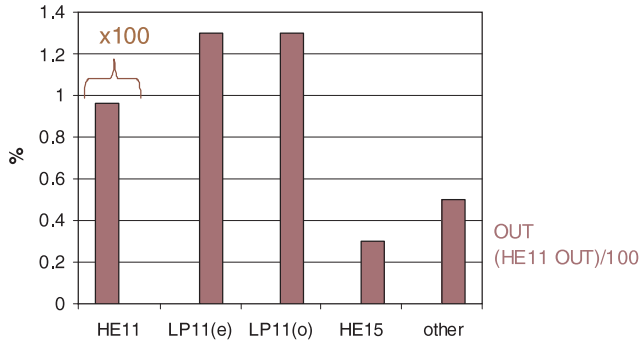

Fig. 6. Percentage of power in the output for the pure HE_{11} mode input in the ITER TL.

The loss components 1, 2, and 3 combine to create calorimetric loss, which is the power loss between the two ports while loss component 4 is associated with other modes appearing in the output port.

The loss in Fig. 5 for the pure HE_{11} mode is similar to the value obtained in previous analysis of the ITER TL loss.[9] We have calculated the loss for a series of pure LP_{mn} modes; only the lowest-order modes are shown in Fig. 5.

Figure 6 shows the output mode content for a pure HE_{11} mode input. As shown in Fig. 5, for the pure HE_{11} mode, the "Loss due to conversion to other modes" is 3.4%. Figure 6 illustrates how this 3.4% of power is distributed among the HOMs. Figure 6 shows that the next mode up from the HE_{11} mode, the LP_{11} mode (odd and even), is the most likely mode to be excited because of mode conversion on the ITER TL.

V. LOSS ON THE ITER TL: RESULTS FOR A MIXTURE OF LP_{mn} MODES

In Sec. IV, we calculated the loss on the ITER TLs for pure LP_{mn} modes. In this section, we consider mixtures of modes. The mixtures considered are those previously labeled cases 2, 3, and 4. However, for completeness and comparison, we will also include case 1, which is a pure mode case. The loss on the ITER TL has three components: coupling loss, mode conversion loss, and ohmic or calorimetric loss. Case 1 is a pure HE_{11} mode, case 2 is a mixture of modes with 3% HOM content, case 3 has 10% HOM content, and case 4 has 20% HOM content. Cases 1 and 2 are ideal examples, while cases 3 and 4 may be more realistic examples.

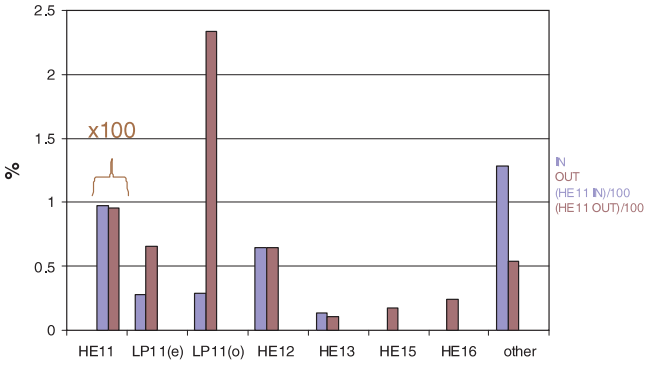

Fig. 7. Percentage of modal power in the input and output for the GB input that is 97% of HE_{11} mode.

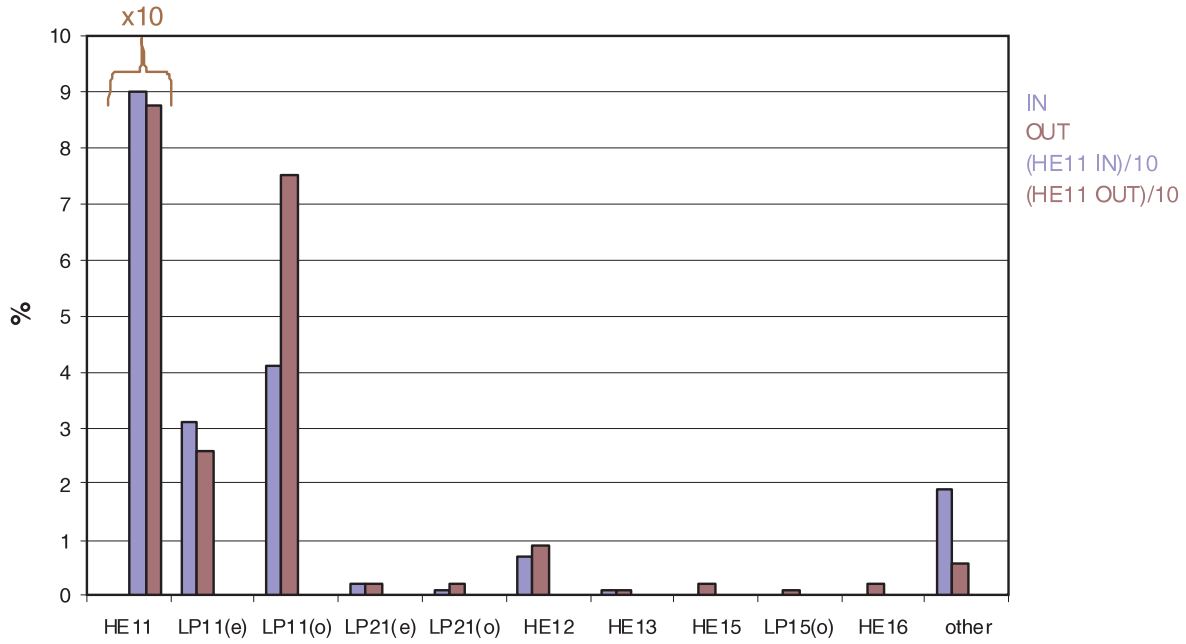

Fig. 8. Percentage of modal power in the input and output for the GB input that is 90% of HE_{11} mode.

V.A. Mode Conversion Loss for a Mixture of LP_{mn} Modes

The results for case 1 were reported in Sec. IV, which treated the case of pure modes. The results for mode conversion for cases 2, 3, and 4 are in Figs. 7, 8, and 9, respectively. Figures 7, 8, and 9 show the mode mixtures on the TL at two locations: at the input port and at the output port. For each mode, the power is reported as the percentage of power in the given LP_{mn} mode divided by the total power in all modes. Figure 7 shows the result for case 2 with 3% HOMs at the input. These results show that there is a modest increase of HOMs at the output port, particularly the LP_{11} modes (even and odd). Figures 8 and 9 show similar behavior for the cases with

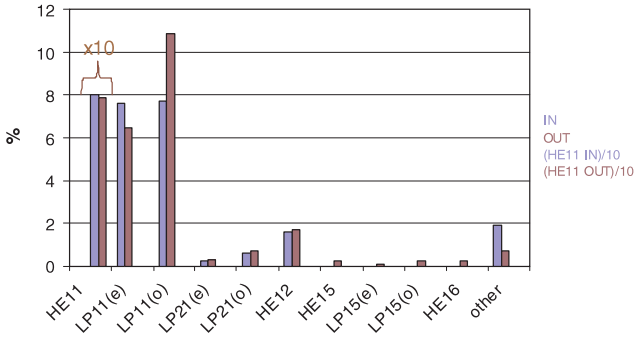

Fig. 9. Percentage of modal power in the input and output for the GB input that is 80% of HE_{11} mode.

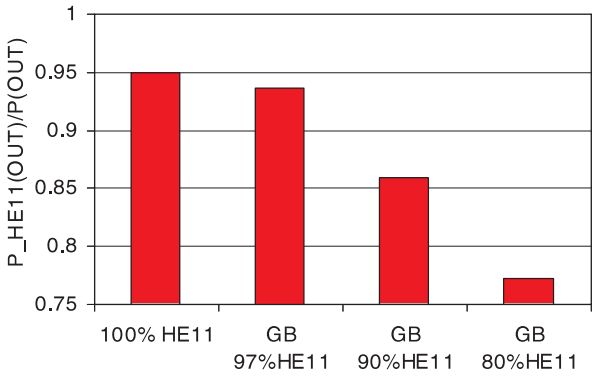

Fig. 10. Output HE_{11} mode content: (a) pure HE_{11} mode input. GB input that is (b) 97% HE_{11}, (c) 90% HE_{11}, and (d) 80% HE_{11}.

larger HOM content at the input port. For clarity, we show in Fig. 10 the fraction of power in the HE_{11} mode at the output port for each of the four cases. The information in Fig. 10 is also evident in Figs. 6 through 9 but is difficult to read in those figures.

V.B. Calculation of Calorimetric Power Loss in the TL

Figure 11 shows the calorimetric loss for the four cases. There are four sources of calorimetric loss:

1. truncation loss. This loss occurs because the nearly GB at the TL input port has a small fraction of power, ~1% as seen in Fig. 11, which is outside

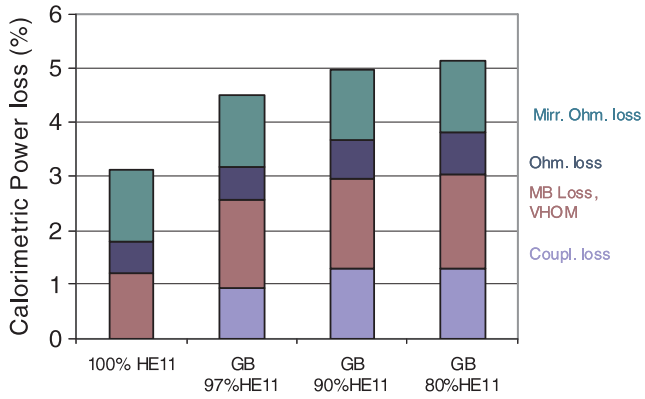

Fig. 11. Calorimetric loss (%) in the ITER TL for (a) pure HE_{11} mode input; (b) GB input that is 97% HE_{11} mode; (c) GB that is 90% HE_{11}; (d) GB that is 80% HE_{11}. Partitions: (1) coupling losses; (2) losses in the MBs due to excitation of VHOMs that add to ohmic losses; (3) ohmic losses in straight sections; (4) ohmic losses in the MB mirrors.

of the 63.5-mm-diam waveguide aperture. In the ideal case, case 1 of a pure HE_{11} mode, this loss is zero.

2. MB loss and VHOMs. This loss is due to the excitation of VHOMs at an MB.
3. ohmic loss in straight sections
4. ohmic loss upon reflection at MB and polarizer mirrors.

Calorimetric loss is distinguished from mode conversion loss. In MBs, significant mode conversion loss occurs in lower-order modes of the waveguide. These modes can transit the entire ITER ECH TL. This can be seen from the results shown for individual modes in Fig. 5. For example, the HE_{13} mode has 30% loss for the entire line, so that the majority of power converted into this mode at MBs would appear at the output port. Mode conversion to VHOMs that are near cutoff results in modes that do not transit the line and thus produce ohmic or calorimetric loss. The code used for these calculations tracks the lowest 110 LP_{mn} modes of the TL and thus accounts with high accuracy for the ohmic loss due to HOMs. Since the HE_{11} mode is the majority of power in each case, the calorimetric loss is similar for all of the cases in Fig. 11. The loss due to VHOM excitation varies from 0.003 to 0.013 dB per bend.

The results in Fig. 11 are consistent with the results for individual modes (Fig. 5) and the modal power plots (Figs. 7, 8, and 9). In fact, the MB VHOM loss for case 2 is 0.07 dB from Fig. 11. Taking the input mode content from Fig. 7 and the MB VHOM loss for individual modes from Fig. 5, we obtain the same loss of 0.07 dB.

VI. SUMMARY OF HE_{11} MODE OUTPUT POWER FOR THE FOUR CASES

The results of the calculations are summarized here. We are interested in the output power that is in the HE_{11} mode in each of the four cases since only the power in the HE_{11} mode will be properly launched into the ITER plasma. The power at the output port that is not in the HE_{11} mode is shown in Fig. 12. The lost power has three main components:

1. coupling loss, which is power that did not couple into the TL at the input port
2. ohmic (calorimetric) loss due to VHOM modes at MBs, straight section ohmic loss, and mirror ohmic loss
3. mode conversion loss due to mode conversion at the MBs and also due to waveguide sag, tilt, and offset at waveguide junctions.

The loss due to sagging, tilt, and offset of straight waveguide sections was estimated by Doane[9] as 0.075 dB (or 1.7% fractional loss). This loss was excluded from Fig. 10 to obtain a clearer result but must be included in Fig. 12 for the total loss estimate. We also include in Fig. 12 the estimated loss for the following components (Fig. 2): one isolation valve, two pumping sections, one window, and one switch in the straight position. This estimated loss is 0.022 dB.

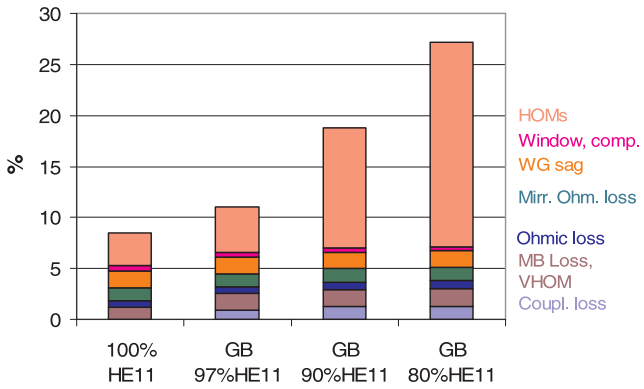

Fig. 12. Percentage of output power that is not in the HE_{11} mode (%) in the ITER TL for (a) pure HE_{11} mode input; (b) GB input that is 97% HE_{11} mode; (c) GB that is 90% HE_{11}; (d) GB that is 80% HE_{11}. Partitions: (1) coupling losses; (2) losses in the MBs due to excitation of VHOMs that add to ohmic losses; (3) ohmic losses in straight sections; (4) ohmic losses in the MB mirrors; (5) HE_{11} mode conversion loss due to sag in waveguide sections and tilt and offset of waveguide section junctions; (6) loss in the window, pumping sections, isolation valve, and the switch in straight position; (7) losses due to HOMs in the output beam.

TABLE VI

Input and Output Power Levels for 1-MW Gyrotron Beam

Case	P_{in} (kW)	P_{in} HE_{11} (kW)	P_{in} HE_{11}/P_{in}	P_{out} (kW)	P_{out} HE_{11} (kW)	P_{out} HE_{11}/P_{out}
1: 100% HE_{11}	1000	1000	1.00	969	920	0.95
2: 97% HE_{11}	991	965	0.97	955	895	0.94
3: 90% HE_{11}	987	886	0.90	950	817	0.86
4: 80% HE_{11}	987	794	0.80	949	732	0.77

The final result of the calculation is also listed in Table VI, which shows the losses for a 1-MW, 170-GHz gyrotron beam on the ITER ECH TL for each case (except for case 1). For the results presented in Table VI, the definition of the parameters is given by

P_{in} (kW) = power injected into TL from the incident 1-MW gyrotron beam

P_{in} HE_{11} (kW) = power at the TL entrance port in the HE_{11} mode

P_{out} (kW) = total power at the TL exit

P_{out} HE_{11} (kW) = power at the TL exit in the HE_{11} mode

calorimetric power loss = $1 - P_{out}$ (kW)/1000

HE_{11} mode loss = $1 - P_{out}$ HE_{11} (kW)/1000

output HE_{11} mode content = P_{out} HE_{11}/P_{out}.

We also show the final results in graphical form in Fig. 13. We see from Table VI and Fig. 13 that for 1 MW of power at the MOU output, the output power in the HE_{11} mode can be roughly estimated as 920 kW times the fraction of input power in the HE_{11} mode. This estimate can be shown from Fig. 13 to be correct to within 1% error for input power fractions of 80 to 100%. A 97% HE_{11} mode purity input is required for a 94% mode purity output; this is a very stringent requirement.

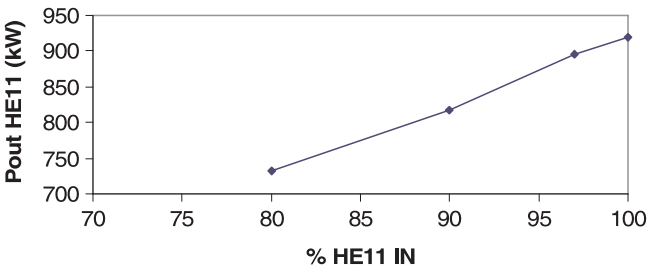

Fig. 13. Output power in the HE_{11} mode versus percentage of HE_{11} in the input.

VII. CONCLUSIONS

The losses on the ITER ECH TL have been calculated for four possible cases corresponding to having HE_{11} mode purity at the input of the TL of 100, 97, 90, and 80%. The losses due to coupling, ohmic, and mode conversion loss are evaluated in detail using a numerical code and analytical approaches. Estimates of the calorimetric loss on the line show that the output power is reduced by about 6, ± 1% because of ohmic loss in each of the four cases. Estimates of the mode conversion loss show that the fraction of output power in the HE_{11} mode is $\sim$3% smaller than the fraction of input power in the HE_{11} mode. High output mode purity therefore can be achieved only with significantly higher input mode purity. Combining both ohmic and mode conversion loss, for 1 MW of power generated by the gyrotron, the output power in the HE_{11} mode at the end of the ITER TL can be roughly estimated as 920 kW times the fraction of input power in the HE_{11} mode.

The loss calculated in this paper is only intended as a representative calculation. Since the design of the ITER TL is not yet fixed, the results may be different for the final TL. However, it is hoped that the present calculation can provide guidance for the expected TL performance under ideal conditions. The present calculations are for an ideal system. A real system will have higher loss than the value calculated here. In a real TL used over a period of time, losses may also increase due to displacement of parts.

ACKNOWLEDGMENTS

The authors would like to thank J. Doane and R. Olstad of General Atomics and M. Henderson of the ITER Organization for helpful discussions.

This research was supported by the U.S. Department of Energy, Office of Fusion Energy Sciences, and by the U.S.

ITER Project managed by Battelle/Oak Ridge National Laboratory.

REFERENCES

1. T. IMAI, N. KOBAYASHI, R. TEMKIN, M. THUMM, M. Q. TRAN, and V. ALIKAEV, "ITER R&D: Auxiliary Systems: Electron Cyclotron Heating and Current Drive System," *Fusion Eng. Des.*, **55**, 281 (2001).

2. M. A. HENDERSON et al., "A Revised ITER EC System Baseline Design Proposal," *Proc. 15th Joint Workshop Electron Cyclotron Emission and Electron Cyclotron Resonance Heating (EC-15)*, p. 458, J. LOHR, Ed., World Scientific Publishing Company, Singapore (2009).

3. S. CIRANT, "Overview of Electron Cyclotron Heating and Electron Cyclotron Current Drive Launcher Development in Magnetic Fusion Devices," *Fusion Sci. Technol.*, **53**, 12 (2008).

4. M. A. HENDERSON et al., "Critical Design Issues of the ITER ECH Front Steering Upper Launcher," *Fusion Sci. Technol.*, **53**, 139 (2008).

5. M. A. HENDERSON and G. SAIBENE, "Critical Interface Issues Associated with the ITER EC System," *Nucl. Fusion*, **48**, *5*, 054017 (May 2008).

6. J. LOHR et al., "The Electron Cyclotron Resonant Heating System on the DIII-D Tokamak," *Fusion Sci. Technol.*, **48**, 1226 (2005).

7. R. A. OLSTAD, J. L. DOANE, and C. P. MOELLER, "ECH MW-Level CW Transmission Line Components Suitable for ITER," *Fusion Eng. Des.*, **74**, *1–4*, 331 (Nov. 2005).

8. J. L. DOANE and R. A. OLSTAD, "Transmission Line Technology for Electron Cyclotron Heating," *Fusion Sci. Technol.*, **53**, 39 (2008).

9. J. L. DOANE, "Design of Circular Corrugated Waveguides to Transmit Millimeter Waves at ITER," *Fusion Sci. Technol.*, **53**, 159 (2008).

10. K. KAJIWARA, K. TAKAHASHI, N. KOBAYASHI, A. KASUGAI, T. KOBAYASHI, and K. SAKAMOTO, "Development of the Transmission Line and the Launcher for the ITER ECH System," *Proc. Joint 32nd Int. Conf. Infrared and Millimeter Waves and the 15th Int. Conf. Terahertz Electronics (IRMMW-THz)*, Cardiff, United Kingdom, September 2–7, 2007, p. 793 (2008).

11. S. T. HAN et al., "Low-Power Testing of Losses in Millimeter-Wave Transmission Lines for High-Power Applications," *Int. J. Infrared Millimeter Waves*, **29**, *11*, 1011 (2008).

12. S. PARK, J. JEONG, W. NAMKUNG, M.-H. CHO, Y. S. BAE, W.-S. HAN, and H.-L.YANG, "Commissioning of KSTAR 84-GHz ECH Transmission System," *Fusion Sci. Technol.*, **55**, 56 (2009).

13. M. CENGHER, J. LOHR, I. A. GORELOV, W. H. GROSNICKLE, D. PONCE, and P. JOHNSON, "Measurements of the ECH Power and of the Transmission Line Losses on DIII-D," *Proc. 15th Joint Workshop Electron Cyclotron Emission and Electron Cyclotron Resonance Heating (EC-15)*, Yosemite, California, March 10–13, 2008, p. 483, J. LOHR, Ed., World Scientific Publishing Company, Singapore (2009).

14. R. A. OLSTAD, R. W. CALLIS, J. L. DOANE, H. J. GRUNLOH, and C. P. MOELLER, "Progress on Design and Testing of Corrugated Waveguide Components Suitable for ITER ECH and CD Transmission Lines," *Proc. 15th Joint Workshop Electron Cyclotron Emission and Electron Cyclotron Resonance Heating (EC-15)*, Yosemite, California, March 10–13, 2008, p. 542, J. LOHR, Ed., World Scientific Publishing Company, Singapore (2009).

15. R. W. CALLIS et al., "Design and Testing of ITER ECH & CD Transmission Line Components," *Fusion Eng. Des.*, **84**, 526 (2009).

16. K. OHKUBO, S. KUBO, H. IDEI, M. SATO, T. SHIMOZUMA, and Y. TAKITA, "Coupling of Tilting Gaussian Beam with Hybrid Mode in the Corrugated Waveguide," *Int. J. Infrared Millimeter Waves*, **18**, *1*, 23 (1997).

17. P. J. B. CLARRICOATS and R. D. ELLIOT, "Multimode Corrugated Waveguide Feed for Monopulse Radar," *IEE Proc. H (Microwaves, Optics and Antennas)*, **128**, *2*, 102 (1981).

18. S. N. VLASOV and M. A. SHAPIRO, "Optimization of Miter Bend for Oversized Corrugated Waveguide," *Radiotekh. Elektron.*, **36**, 2322 (1991) (in Russian).

19. T. GRAUBNER, W. KASPAREK, and H. KUMRIC, "Optimization of Coupling Between HE_{11}-Waveguide Mode and Gaussian Beam," *Proc. 18th Int. Conf. Infrared and Millimeter Waves*, Colchester, United Kingdom, September 6–10, 1993, p. 477, Springer, New York (1993).

20. M. THUMM and W. KASPAREK, "Passive High-Power Microwave Components," *IEEE Trans. Plasma Sci.*, **30**, 755 (2002).

21. W. KASPAREK, A. FERNANDEZ, F. HOLLMANN, and R. WACKER, "Measurement of Ohmic Loss of Metallic Reflectors at 140 GHz by a 3-Mirror Resonator Technique," *Int. J. Infrared Millimeter Waves*, **22**, 1695 (2001).

22. J. L. DOANE and C. P. MOELLER, "HE_{11} Bends and Gaps in a Circular Corrugated Waveguide," *Int. J. Electron.*, **77**, 489 (1994).

23. E. A. J. MARCATILI, "Miter Elbow for Circular Electric Mode," *Proc. Symp. Quasi-Optics*, p. 535, New York, 1964, Polytechnic Press, Polytechnic Institute of Brooklyn, Brooklyn, New York (1964).

24. D. S. TAX, E. N. COMFOLTEY, S.-T. HAN, M. A. SHAPIRO, J. R. SIRIGIRI, R. J. TEMKIN, and P. P. WOSKOV, "Mode Conversion Losses in ITER Transmission Lines," *Proc. 33rd Int. Conf. Infrared, Millimeter and Terahertz Waves (IRMMW-THz 2008)*, Pasadena, California, September 15–19, 2008, Institute of Electrical and Electronics Engineers (2008).